PERGAMON

Chemical Engineering Science 57 (2002) 4595–4604

Chemical Engineering Science

www.elsevier.com/locate/ces

Design and optimization of catalysts and membrane reactors for the non-oxidative conversion of methane

Lin Li[a,b], Richard W. Borry[a,b], Enrique Iglesia[a,*]

[a] *Department of Chemical Engineering, University of California at Berkeley, 94720-462 Berkeley, CA, USA*
[b] *Division of Materials Sciences, E.O. Lawrence Berkeley National Laboratory, Berkeley, CA 94720, USA*

Received 26 March 2001; received in revised form 19 June 2002; accepted 20 June 2002

Abstract

Kinetic-transport simulations were used in order to explore the relevant thermodynamic and kinetic barriers in the non-oxidative conversion of CH_4 in a membrane reactor and the effects of continuous hydrogen removal and of catalytic sites on CH_4 conversion and on the attainable yields of useful C_2–C_{10} products. A sensitivity analysis of homogeneous CH_4 pyrolysis pathways showed that sites that activate methane to form methyl radicals or ethene and the conversion of ethene to aromatics increased pyrolysis rates, but led to impractical reactor residence times with or without H_2 removal. Catalysts, such as Mo/H-ZSM5, which increase the rate of both CH_4 conversion to ethene and of ethene aromatization are required in order to overcome the kinetic barriers in homogeneous pyrolysis pathways. Homogeneous models were modified by incorporating non-elementary catalytic steps with rate constants obtained from experimental residence time studies on Mo/H-ZSM5. Simulations using this homogeneous–heterogeneous kinetic model were used in order to determine the benefits of continuous H_2 removal on the yields of desired C_2–C_{10} hydrocarbons and on the required residence times and to obtain rigorous criteria for the design of catalysts and membranes for direct methane conversion reactions. Bifunctional catalysts able to catalyze the required steps and the removal of H_2 across ceramic membranes can lead to almost complete CH_4 conversion at $\sim$ 1000 K at practical reactor residence times (< 100 s). This performance requires catalytic reactors with intermediate values of the ratio of characteristic reaction and permeation times ($\delta = 1$–10), which in turn require the use of thin dense ceramic films (10–100 μm) in order to achieve these δ values for practical reactor diameters.

Keywords: Methane; Pyrolysis; Kinetics; Simulation; Reaction engineering; Membranes

1. Introduction

The direct conversion of methane to fuels and petrochemicals remains a formidable challenge. With the exception of processes for producing synthesis gas intermediates via steam reforming and partial oxidation, direct CH_4 conversion reactions remain economically unattractive. For example, oxidative coupling of methane (OCM) (Keller & Bhasin, 1982; Ito & Lunsford, 1985; Tonkovich, Carr, & Aris, 1993; Jiang, Yentekakis, & Vayenas, 1994) yields $< 25\%$ C_2 yields and significant lower yields of ethene, because ethane is the initial coupling product and the activation of C–H bonds in both methane and ethane occurs concurrently with unselective and highly exothermic reactions using O_2 co-reactants to form CO and CO_2. (Labinger, 1988; Reyes, Iglesia, & Kelkar, 1993). Non-oxidative reactions of methane to form aromatics occur on cation-modified zeolites at relatively low temperatures ($\sim$ 1000 K) with low carbon and tar yields, because active sites activate methane within shape-selective environments that restrict chain growth and the formation of polynuclear aromatics (Wang, Tao, Xie, & Xu, 1993; Solymosi, Erdohelyi, & Szoke, 1995; Wang, Lunsford, & Rosynek, 1996; Lunsford, Rosynek, & Wang, 1995, Borry, Kim, Huffsmith, Reimer, & Iglesia, 1999). In contrast, homogeneous methane pyrolysis pathways require much higher temperatures and lead to high selectivities to acetylene and to large polynuclear aromatics. The highly endothermic nature of methane conversion to aromatics, however, leads to very low equilibrium conversions and to benzene yields of only $\sim$ 7% at the low temperatures (950 K) required for selective chain growth. C_2–C_{10} hydrocarbon selectivities as high

* Corresponding author. Tel.: +1-510-642-9673; fax: +1-510-642-4778.
E-mail address: iglesia@cchem.berkeley.edu (E. Iglesia).

0009-2509/02/$ - see front matter
PII: S0009-2509(02)00314-7

as 80% have been reported at near-equilibrium conversions on Mo/H-ZSM5 (Wang et al., 1996). H_2 is formed during methane pyrolysis and it inhibits the forward reaction rates of both catalytic and homogeneous pyrolysis pathways. Hydrogen transport membranes can remove the thermodynamic and kinetic hurdles imposed by the accumulation of H_2 non-oxidative methane reactions (Andersen, Dahl, Jens, Rytter, & Slagtern, 1989; Woldman & Sokolovskii, 1991; Hamakawa, Hibino, & Iwahara, 1993; Hamakawa, Hibino, & Iwahara, 1994; Langguth, Dittmeyer, Hofmann, & Tomandl, 1997). The coupling of methane conversion reactions with hydrogen removal via selective membrane walls poses significant design, optimization, and fabrication issues. The first two issues and the guidance required for the third can be addressed by simulations using reaction kinetic and thermodynamic data together with rigorous descriptions of membrane transport and of reactor hydrodynamics.

A previous report described reaction-transport models for homogeneous methane pyrolysis reactions, including their coupling with a simple surface-catalyzed initiation step leading to methyl radicals (Li, Borry, & Iglesia, 2001). The coupling of these homogeneous pathways (Dean, 1990) with H_2 permeation through the reactor walls led to higher CH_4 reaction rates, mostly as a result of the removal of thermodynamic constraints in the near-equilibrium region, and to C_2–C_{10} yields of ~90% at intermediate values of the dimensionless ratio of characteristic H_2 transport and CH_4 reaction rates ($\delta = 1$–10). H_2 removal, however, did not influence the slow irreversible initiation steps that initially form radicals or the faster steps in the productive chain transfer region, and lead to impractical residence times and reactor volumes. Here, we use reaction-transport simulations in order to probe the identity of rate-determining steps in homogeneous CH_4 pyrolysis and to propose specific catalytic steps required in order to overcome the significant kinetic barriers inherent in these homogeneous pyrolysis pathways, even when initiated by heterogeneous methyl radical generation steps. Specifically, we combine experimental kinetics for shape-selective bifunctional catalysts developed in a parallel experimental effort (Borry et al., 1999; Kim, Borry, & Iglesia, 2000) with homogeneous kinetic models and hydrodynamic descriptions of tubular membrane reactors. The resulting simulations are used to describe the effects of hydrogen removal on hydrocarbon yields and on required residence times and to obtain rigorous criteria for the design of catalyst and membrane materials for the direct conversion of methane to higher hydrocarbons.

2. Kinetics and simulation methods

The rates of homogeneous methane pyrolysis reactions and of hydrogen permeation are described by kinetic and transport equations reported previously (Li et al., 2001) and only a brief description is included here. For complex networks involving n reactions and m components, the rate of reaction for component j is given by

$$R_j = \sum_{i=1}^{n} \lambda_{ij} k_i(T, p) f_i(K, p), \tag{1}$$

where λ_{ij} is the stoichiometric coefficient for species j in reaction i, T is the reaction temperature, K is the equilibrium constant vector, p is the partial pressure vector of the reaction mixture, and k_i and f_i are the rate constant and the dimensionless rate expression for reaction i, respectively. The hydrogen transport flux through the reactor wall is assumed to be proportional to the H_2 partial pressure gradient across the membrane:

$$J_{H_2} = \frac{P}{l}(p_{H_2,1} - p_{H_2,2}), \tag{2}$$

where P is the permeability of H_2 through the membrane, l is the membrane thickness, and $p_{H_2,1}$ and $p_{H_2,2}$ are the H_2 partial pressures on the feed and permeate sides of the membrane, respectively. Certain membrane systems may obey modified versions of Eq. (2), but the use of the appropriate equation in such cases will not alter the trends and the concepts described here using Eq. (2) as a specific example.

In a plug-flow tubular reactor with permselective walls, differential mole balances on the reaction and permeation channels give the dimensionless differential equations

$$\frac{1}{Da}\frac{d\phi_j}{d\xi} = \sum_{i=1}^{n} \lambda_{ij}\beta_i f_i(K, p) - \delta\alpha_j(y_{jt} - y_{js}) \quad \text{(reaction side)}, \tag{3}$$

$$\frac{1}{Da}\frac{dq_j}{d\xi} = \delta\alpha_j(y_{jt} - y_{js}) \quad \text{(permeation side)}. \tag{4}$$

Several dimensionless parameters (Da, δ, α_i and β_i) arise from the non-dimensionalization of these mole balances. These are defined as

$$Da = Lk/F_{10} \quad (\textit{Damkohler number, reactant conversion rate/reactant inlet rate}), \tag{5}$$

$$\delta = \frac{4P_f P_T}{dlk} \quad (\textit{Rate ratio, permeation rate/reaction rate}), \tag{6}$$

$$\alpha_j = P_j/P_f, \tag{7}$$

$$\beta_i = k_i/k_1. \tag{8}$$

Da is a Damkohler number, which reflects the probability of the reaction as the ratio of the reactor residence time to the characteristic reaction time. The parameter δ accounts for the ability of the reactor to transport H_2 and to convert CH_4, as the ratio of the characteristic times for reaction and for H_2 transport.

The dimensionless parameters, Da, δ, α_i and β_i, are defined in terms of a basis reactant, chosen here as CH_4. The consequences of H_2 removal are explored by defining the parameter δ as the ratio of characteristic H_2 transport and CH_4 conversion molar rates. For homogeneous pyrolysis, methane conversion rates are described by a complex kinetic network, and the rate constant (k) required to define Da and δ is not apparent by inspection. In this case, we use a pseudo-first-order rate constant, k_{eff}, obtained by fitting simulated rates using a first-order expression (Li et al., 2001). For catalytic reaction pathways, the reaction rate is expressed per unit catalyst mass, and such rates are converted to a reactor volume basis in the equation for δ by using the catalyst bed density in the packed bed reactor.

Simulations were carried out using CHEMKIN II and DVODE subroutines (Kee, Rupley, & Miller, 1990). Homogeneous kinetic models and rate constants for each elementary step are identical to those reported previously (Li et al., 2001). The catalytic conversion of methane on Mo/H-ZSM5 was simulated by inserting non-elementary catalytic steps into the kinetic network, as described below. The required rate constants for Mo/H-ZSM5 catalysts were obtained using error minimization techniques from the experimental effects of effective reactor residence time on reaction rates and selectivities (Borry, 1998).

3. Results and discussions

3.1. Effect of catalytic pathways on the conversion of C_2H_4 to C_6H_6

Homogeneous methane pyrolysis reactions exhibit three kinetic stages (Fig. 2 in Li et al., 2001):

(i) an induction period ($t \sim 2400$ s, $T = 1038$ K), during which CH_4 conversion is limited by slow initiation steps ($CH_4 \overset{k_{h1}}{=} CH_3\cdot + H\cdot$),
(ii) a chain transfer regime reached as $CH_3\cdot$ and $H\cdot$ radicals accumulate and reach pseudosteady-state and within which most of the CH_4 conversion occurs,
(iii) a near-equilibrium stage within which most elementary steps (and the overall reaction) become unproductive as they reach thermodynamic equilibrium.

The coupling of homogeneous pyrolysis with H_2 permeation through reactor walls led to higher CH_4 reaction rates at high methane conversions (stage (iii)), mostly as a result of the removal of the prevalent thermodynamic constraints near equilibrium. H_2 removal, however, did not influence the slow irreversible initiation steps that initially form radicals or the faster steps in the productive chain transfer region, within which most of the chemical conversion occurs; therefore, reactor residence times and volumes remained impractically large.

The introduction of a surface-catalyzed initiation step

$$CH_4 + [^*] \overset{k_{s1}}{\rightarrow} CH_3\cdot + [^*H] \quad (9)$$

increased methane conversion rates at low conversions by replacing the homogeneous version of this step with a faster step, which rapidly forms the radicals required to enter the chain transfer regime. The effects of these surface steps can be explored by introducing a dimensionless parameter $\rho = k_{s1}/k_{h1}$, which reflects the relative contributions of catalytic (k_{s1}) and homogeneous (k_{h1}) methyl radical generation steps. Induction periods become shorter with increasing ρ, but chain transfer rates and near-equilibrium conversion rates are largely unaffected by surface-catalyzed initiation steps. Also, product distributions were essentially unaffected by heterogeneous methyl radical formation processes, because CH_4 conversion occurs predominately in the chain transfer region, within which radical concentrations and reaction rates are controlled by homogeneous chain transfer steps.

The continuous removal of H_2 along a tubular reactor increased CH_4 reaction rates by removing the molecules required for unproductive reverse reactions as individual steps approach equilibrium. Therefore, methyl radical formation on surfaces cannot increase chain transfer rates, which are required in order to convert radicals into stable reaction products. Surface sites that replace these chain transfer steps are required in order to overcome the intrinsic kinetic barriers imposed by these homogeneous pathways. The attainment of the high C_2–C_{10} yields achievable with continuous H_2 removal within practical residence times will require catalytic sites that also convert the initial C_2 products formed via homogeneous recombination of methyl radicals into more stable aromatics. The predominant CH_4 pyrolysis products are ethene, benzene, and naphthalene at 823–1073 K. Thus, we may refer to their inter-conversion using the non-elementary steps in Scheme 1 in order to discuss the behavior of the overall reaction, even when the simulations rigorously include the detailed steps included in the complete kinetic network throughout.

The rigorous monitoring of the approach to equilibrium for homogeneous or catalyst-initiated reaction networks showed that step 1 approaches equilibrium within the chain transfer region and the overall reaction becomes limited by largely irreversible steps that convert ethene to aromatics. The net forward rate of methane conversion reaction and the product distribution in the chain transfer regime, within which most of the conversion occurs, become controlled by the rate of C_2H_4 conversion to products (via steps 2–4). In the absence of a catalyst for this reaction, these reactions occur only via homogeneous routes.

The quasi-equilibrated nature of the initial CH_4 to C_2H_4 reaction requires that one of the products of this reaction be “scavenged” in order to overcome thermodynamic constraints. One approach involves the removal of the H_2 formed using a membrane (Borry, Lu, Kim, & Iglesia, 1998, Li et al., 2001). Another approach would react C_2H_4 in an

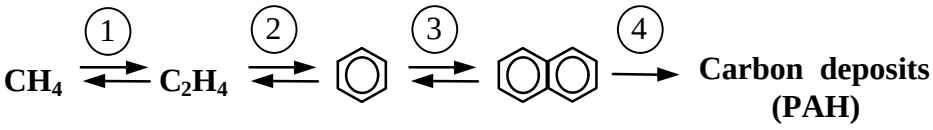

Scheme 1. Consecutive reaction steps for methane conversion.

efficient reaction to form aromatic molecules, which are favored by thermodynamics and are present in concentrations well below equilibrium values in the absence of such conversion pathways. Here, we first explore the role of catalytic ethene conversion pathways using a conceptual reaction scheme without H_2 removal. Then, we replace this scheme with one appropriate for available Mo/H-ZSM5 catalysts. Finally, in the last section we couple these realistic catalytic kinetics with continuous H_2 removal in a tubular reactor.

Catalytic C_2H_4 conversion pathways are first described here by introducing the following non-elementary catalytic reaction steps:

$$3C_2H_4 = C_6H_6 + 3H_2. \tag{10}$$

The reaction rate is assumed to obey the rate expression

$$r_2 = k_2 C_{C_2H_4}(1 - \eta_2) \tag{11}$$

in which the approach to equilibrium for this step (η_2) is described by

$$\eta_2 = \frac{C_{C_6H_6} \cdot C_{H_2}^3}{C_{C_2H_4}^3} \frac{1}{K_2} \tag{12}$$

and k_2 and K_2 are the reaction rate constant and equilibrium constant of reaction (6), respectively.

Figs. 1 and 2 show the effects of catalytic ethene conversion rates on CH_4 conversion and on the approach to equilibrium for CH_4 conversion to C_2H_4. The parameter γ is given by the ratio of the first-order rate constants for ethene conversion to benzene (k_2 in Eq. (11)) and for methane conversion (k_{eff}). The value of η_1 in Fig. 2 reflects the approach to equilibrium for the CH_4–C_2H_4 reaction (step 1 in Scheme 1) and it is defined as

$$\eta_1 = \frac{C_{C_2H_4} \cdot C_{H_2}^2}{C_{CH_4}^2} \cdot \frac{1}{K_1}, \tag{13}$$

where K_1 is the equilibrium constant for the reaction

$$2CH_4 = C_2H_4 + 2H_2. \tag{14}$$

Fig. 2 shows that step 1 approaches equilibrium quickly in the absence of ethene to benzene conversion catalytic pathways ($\gamma = 0$), and η_1 becomes greater than 90% at CH_4 conversions of $\sim$ 10%. The approach to equilibrium is very similar for purely homogeneous and for catalytically initiated homogeneous pyrolysis pathways (Fig. 2), because initiation steps do not contribute to reaction rates in the chain transfer regime, within which the approach to equilibrium occurs. Catalytic initiation pathways decrease the residence time required to reach a given conversion by eliminating the induction period imposed by slow homogeneous initiation processes (Fig. 1). Changes in conversion with residence time become very small as the CH_4 conversion to C_2H_4 reaches equilibrium values, because the higher equilibrium conversions possible as ethene is converted to benzene are

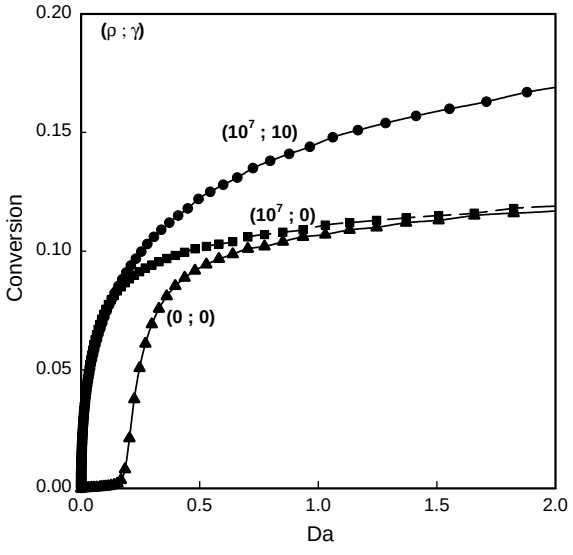

Fig. 1. Comparison of methane conversion via homogeneous reaction, catalytic formation of CH_3, and catalytic conversion of C_2H_4 to benzene (1038 K).

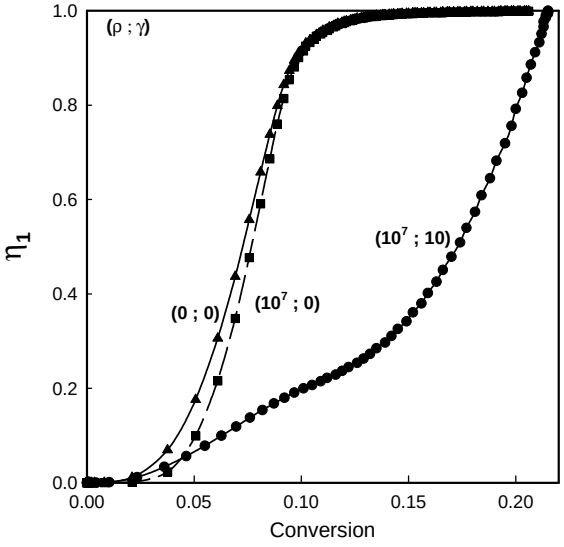

Fig. 2. Approach to equilibrium of methane to ethene step with various values of δ and γ (1038 K).

achieved only via slow homogeneous pathways when catalytic sites are not available ($\gamma = 0$).

The introduction of catalytic sites (γ=10) decreases the value of η_1 for CH_4 conversion to C_2H_4 by continuously removing the ethene formed in this reaction (Fig. 2). This continuous removal of ethene also eliminates the asymptotic conversion limit reached in the absence of heterogeneous pathways (γ=0; Fig. 1). Such catalytic sites, however, do not influence reaction rates in the chain transfer kinetic regime (Fig. 1), because CH_4 conversion to C_2H_4 is far from equilibrium at low CH_4 conversion. Thus, the residence times required for γ values of 10 are only slightly lower than those for purely homogeneous ethene to benzene conversion pathways. High methane conversions at short contact times will require catalytic sites that increase the rates of ethene formation from methane and of ethene conversion to aromatics.

Many elementary homogeneous steps are involved in the synthesis of C_2H_4 from CH_4. We have carried out a sensitivity analysis of the homogeneous reaction pathways by increasing the rate constants of individual elementary steps in order to identify the rate-determining steps. This allows the selective introduction of specific catalytic sites in order to carry such steps more rapidly and to overcome the kinetic bottlenecks imposed by homogeneous pathways. This sensitivity analysis showed that a catalytic pathway for the synthesis of C_2H_4 from CH_4 is required for practical reactor volumes at the low temperatures suitable for selective pyrolysis pathways. Neither CH_3 radical generation nor ethene to benzene catalytic sites are sufficient for practical reaction rates, because overall methane conversion rates ultimately become limited by homogeneous recombination of CH_3 radicals to form C_2H_6 or by the subsequent dehydrogenation of C_2H_6 to form C_2H_4. Neither one of these steps is sufficiently fast to match the typical rates of the catalytic conversion of ethene to benzene.

Active sites that catalyze methane activation to form CH_3 radicals will also catalyze C_2H_6 dehydrogenation to form C_2H_4. We can include the effects of this reaction as an elementary step for C_2H_6 activation in the heterogeneous kinetic model with a rate constant estimated using a modified Evans–Polanyi correlation (Borry, 1998):

$$C_2H_6 + [^*] \xrightarrow{k_{s2}} C_2H_5 \cdot + [^*H]. \quad (15)$$

Fig. 3 gives the methane conversion obtained by considering catalytic activation of CH_4 and C_2H_6 ($\rho = 10^7$, and k_{s2}/k_{s1}=6) and the catalytic conversion of ethene to benzene ($\gamma = 10$). The methane conversion rate is much lower than that experimentally measured on Mo/H-ZSM5 catalysts, and a further increase in the value of ρ did not influence methane conversion rates, which are limited by the recombination of CH_3 to form C_2H_6. This was confirmed by the higher rates obtained by artificially increasing the reaction rate for CH_3 recombination steps (Fig. 3).

Several studies have addressed the reaction pathways for CH_4 conversion to aromatics on Mo/H-ZSM5 (Chen, Lin, Xu, Zhang, 1995, Wang et al., 1996; Solymosi, Cserenyi, Szoke, Bansagi, Oszko, 1997; Borry et al., 1999; Ding, Li, Meitzner, & Iglesia, 2001). Some studies have proposed that ethene forms via homogeneous recombination of CH_3 radicals produced by C–H activation on catalytic sites (Chen et al., 1995), as found earlier for oxidative coupling of methane on oxide catalysts. Our simulations show that purely homogeneous CH_3 recombination pathways cannot account for the observed rate of CH_4 conversion on Mo/H-ZSM5, even for arbitrarily fast heterogeneous CH_3 radical formation steps. Therefore, active sites for both methane conversion to ethene and for ethene cyclodimerization reactions to form aromatics are required in order to reach practical methane conversions in reasonable residence times.

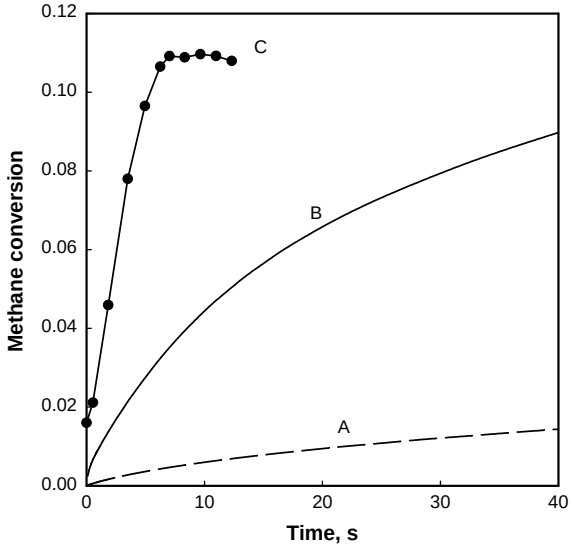

Fig. 3. Comparison of methane conversion on Mo/H-ZSM5 catalyst with the maximum possible value through homogeneous recombination of CH_3 radical to form C_2H_6. A: Homogeneous pyrolysis with catalytic pathways for CH_4 and C_2H_6 activation and for ethene to benzene conversion (1038 K). B: Same conditions as A but rate constant for CH_3 recombination to form C_2H_6 higher by a factor of 10^5. C: Experimental data on 4 wt %. Mo/H-ZSM5 catalyst (950 K).

3.2. *Simulation of the rate and selectivity of catalytic methane conversion on Mo/H-ZSM5*

The requirement for catalysts that:

(i) break C–H bonds in CH_4 (and in any higher alkanes formed) to form CH_x surface fragments,
(ii) recombine CH_x groups to form at least C_2 hydrocarbons, and
(iii) oligomerize and cyclize alkenes into thermodynamically favored aromatics

is likely to require metal-like surfaces for steps (i) and (ii) and acid sites for step (iii). Oligomerization and cyclization pathways unconstrained by shape-selective channels, such as those provided by medium-pore pentasil zeolites, however, lead to polynuclear aromatic molecules at the temperatures

required for C–H bond activation in CH_4. Mo/H-ZSM5 catalysts appear to satisfy these requirements. These materials catalyze CH_4 conversion to aromatics via bifunctional pathways, with near-equilibrium yields of benzene and $> 80\%$ selectivity to C_2–C_{10} hydrocarbons at ~ 1000 K (Wang et al., 1993; Solymosi et al., 1995; Wang, et al., 1996; Lunsford et al., 1995, Borry et al., 1999).

Our kinetic studies of CH_4 reactions on Mo/H-ZSM5 have confirmed the earlier proposal (Lunsford et al., 1995) that aromatization involves the sequential formation of ethene (and possibly ethane) on MoC_x clusters (formed from exchanged MoO_x precursors during reaction). This initial step is followed by the conversion of ethene and ethane to aromatics via bifunctional pathways on acid sites aided by hydrogen desorption from MoC_x sites. Ethane–ethene equilibrium appears to be maintained throughout the experimental conversion range; therefore, we group both C_2 molecules rigorously into one kinetic lump. These consecutive reactions are similar to those shown previously in Scheme 1, and the rate equations for each reaction are shown in Eqs. (16)–(22) for Mo/H-ZSM5 catalysts.

Step 1:

$$2CH_4 = C_2H_4 + 2H_2, \tag{16}$$

$$r_1 = k_1 C_{CH_4}(1 - \eta_1). \tag{17}$$

Step 2:

$$3C_2H_4 = C_6H_6 + 3H_2, \tag{18}$$

$$r_2 = k_2 C_{C_2H_4}(1 - \eta_2). \tag{19}$$

Step 3:

$$C_6H_6 + 2C_2H_4 = C_{10}H_8 + 3H_2, \tag{20}$$

$$r_3 = k_3 C_{C_2H_4} C_{C_6H_6}(1 - \eta_3), \tag{21}$$

$$\eta_3 = \frac{C_{C_{10}H_8} C_{H_2}^3}{C_{C_2H_4}^2 C_{C_6H_6} K_3}. \tag{22}$$

The rate constants, k_1, k_2 and k_3, in these equations were estimated from experimental residence time effects on rates of formation of individual products. The equilibrium constants, K_1, K_2 and K_3 were calculated using literature thermodynamic data (Li et al., 2001). Fig. 4 compares experimental and simulated product selectivities as a function of CH_4 conversion, which was varied by changing the reactor residence time at constant temperature (950 K) and inlet CH_4 partial pressure (0.5 bar) and by allowing the number of sites within the reactor to decrease as deactivation occurs. The values giving the best fit for k_1, k_2 and k_3 were 0.04 s^{-1}, 4.2 s^{-1}, and 1.2×10^7 cm^3 mol^{-1} s^{-1}. This simple, but mechanistically reasonable, set of rate expressions adequately describes CH_4 reaction pathways on

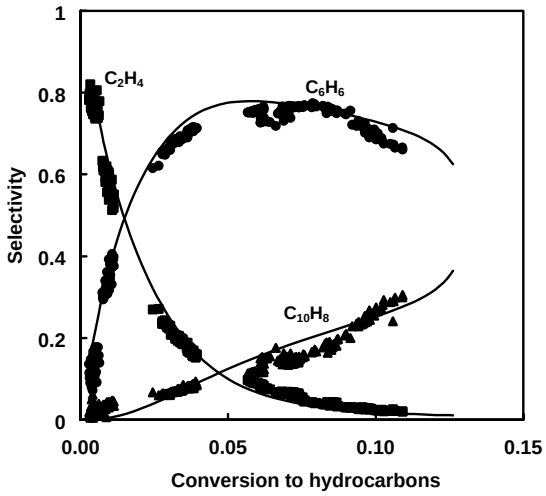

Fig. 4. Simulation and experimental results on Mo-H-ZSM5 catalyst (950 K, 0.5 atm CH_4).

Mo/H-ZSM5. H_2addition experiments have shown inhibition of CH_4 conversion rates consistent with the approach to equilibrium rigorously contained within the kinetic model described above. These experiments, however, also detected kinetic inhibition effects of H_2, which lead to lower pseudo-first order rate constants for each of the steps as H_2 concentrations increase. The kinetic model used here neglects these kinetic inhibition effects; as a result, it will also neglect the additional kinetic benefits of hydrogen removal and underestimate the reaction rate improvements achieved by the continuous removal of H_2 along an actual catalytic reactor.

3.3. *Effect of hydrogen removal on catalytic CH_4 conversion on Mo/H-ZSM5*

The kinetic model for catalytic CH_4 conversion on Mo/H-ZSM5 was coupled with a hydrodynamic model for a tubular reactor with hydrogen-permeable walls (Eqs. (4) and (5)). The catalytic pathways used (Eq. (16)–(22)) can complete the conversion of methane to ethene, benzene, and naphthalene much faster than corresponding homogeneous pathways. Nevertheless, the entire homogeneous kinetic network (Li et al., 2001) was included in the simulations in order to detect any coupling between homogeneous and heterogeneous pathways and to provide a homogeneous path for the formation of polynuclear aromatics via acetylene chain growth steps that occur in the gas phase. Figs. 5–8 show the results of these simulations of heterogeneous and homogeneous reactions in a tubular reactor with continuous H_2 removal. The results are shown for a wide range of the Damkohler number ($Da = 0$–10) and of the ratio of characteristic times for reaction and transport ($\delta = 10^{-3}$–10^2). In these simulation results, the rate constant k_1 for the methane to ethene step (Eq. (16)) is used to define the dimensionless parameters Da and δ after converting the rate constant to a volumetric basis.

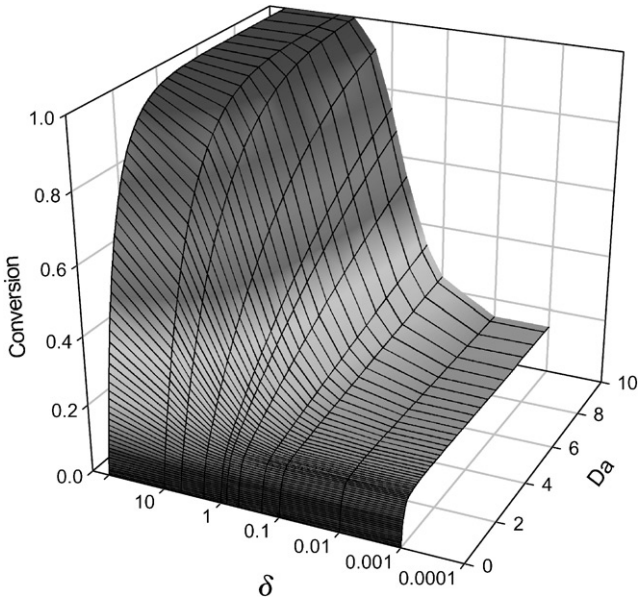

Fig. 5. Methane conversion on Mo/H-ZSM5 catalyst with hydrogen removal (950 K).

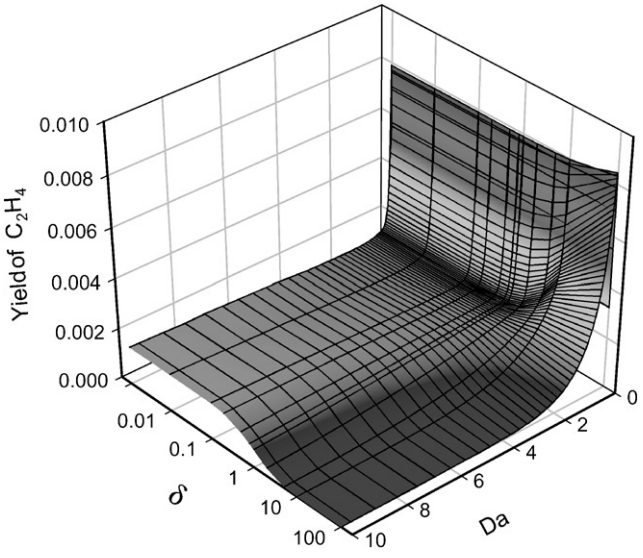

Fig. 6. Ethene yield on Mo/H-ZSM5 catalyst with hydrogen removal (950 K).

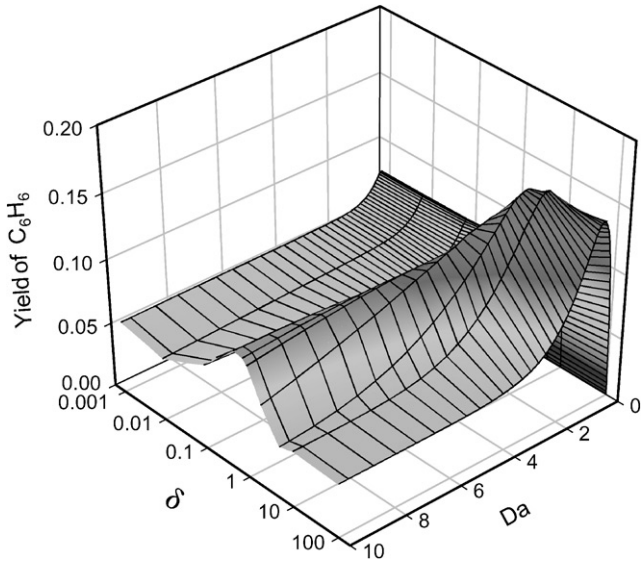

Fig. 7. Benzene yield on Mo/H-ZSM5 catalyst with hydrogen removal (950 K).

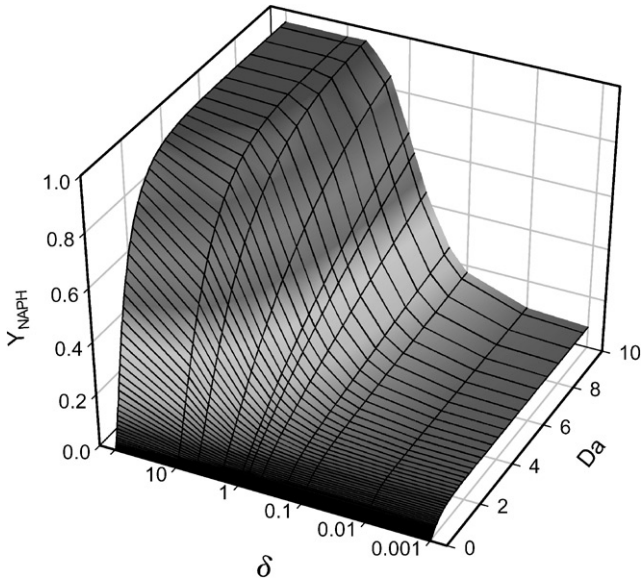

Fig. 8. Naphthalene yield on Mo/H-ZSM5 catalyst with hydrogen removal (950 K).

For a given value of *Da*, CH_4 conversion increases monotonically with increasing δ values, as a result of the removal of thermodynamic constraints for each one of the heterogeneous steps as H_2 is removed. Conversely, the value of *Da* required to reach a given CH_4 conversion decreases with increasing δ, as a result of a higher net forward rate of all three reactions as H_2 concentrations decrease. As also found for homogeneous pyrolysis simulations (Li et al., 2001), the effects of H_2 removal become detectable for δ values between 0.1 and 10. Values of δ larger than 10 lead to negligible H_2 concentrations at all residence times. Values of δ smaller than 0.1 remove negligible amounts of H_2 and do not influence local H_2 concentrations within the reactor.

In general, the results shown in Figs. 5–8 are similar to those for purely homogeneous pathways (Li et al., 2001). For a given value of *Da*, however, homogeneous and heterogeneous pathways obviously require different reactor residence times, because catalytic pathways provide a much larger first-order kinetic rate constant for the kinetically relevant steps ($k_1 = 4 \times 10^{-2}\ s^{-1}$) than homogeneous pathways ($k_{eff} = 7 \times 10^{-5}\ s^{-1}$). Catalytic steps that provide a complete path from CH_4 to aromatics eliminate the kinetic

barriers that prevent practical methane conversions at short contact times. For example, CH_4 conversions of $\sim 90\%$ can be reached for Da values of 4 and δ values of 10. These correspond to residence times of ~ 100 s. As discussed below, the higher reaction rates achievable via these catalytic pathways require correspondingly higher H_2 permeation rates in order to attain the required values of δ.

At low CH_4 conversions and short residence times ($Da \ll 1$), H_2 removal increases C_2 yields (Fig. 6), but these yields then decrease at higher contact times (Da), because the continuous removal of H_2 favors also the subsequent conversion of ethene to aromatics. Benzene yields (Fig. 7) show a maximum as the H_2 removal rate increases, because benzene is also ultimately converted to naphthalene (and ultimately to larger aromatics via homogeneous pathways). At high values of δ and Da, the reaction proceeds completely to the final product (naphthalene), which then converts slowly to larger polynuclear aromatics via homogeneous routes. Our heterogeneous kinetic model does not explicitly include coke formation steps. The homogeneous kinetic model includes H-abstraction/C_2H_2-addition steps that lead to the formation of polynuclear aromatic hydrocarbons (PAH). In order to probe the effect of catalytic sites on the potential formation of acetylene via C–H bond activation in ethene, we introduced such pathways with a rate constant chosen based on the C–H bond energy in ethene and the Evans–Polanyi relations described previously (Borry, 1998). The simulations show that ethene conversion to acetylene reaction approaches equilibrium even for purely homogeneous pathways. Thus, catalytic pathways do not increase the effectiveness of homogeneous PAH formation steps or produce acetylene more efficiently than purely homogeneous steps. Homogeneous H-abstraction/C_2H_2-addition reactions are slower compared with catalytic formation rates for benzene and naphthalene; therefore, naphthalene yields approach 100% as H_2 removal rates increase (Fig. 8).

This simplified kinetic model cannot address the effect of H_2 removal on catalytic pathways for coke formation, which is a slow but detectable process on Mo/H-ZSM5 catalysts. The maximum attainable C_2–C_{10} hydrocarbon yields will ultimately depend on the relative effects of H_2 concentration on the formation of these products and on their subsequent conversion to larger aromatics and coke, a step that appears to be inhibited by the shape-selective environment within zeolite channels. These simulation results (Figs. 5–8) suggest that bifunctional catalysts, such as Mo/H-ZSM5 and continuous H_2 removal can lead to near complete conversions of CH_4. These simulations suggest that very high C_6–C_{10} yields can be achieved in these catalytic membrane reactors in the absence of significant chain growth beyond naphthalene.

The results described above suggest that δ values between 1 and 10 are required in order to attain high conversions and high C_2–C_{10} yields. The defining equation for δ (Eq. (6)) shows that for a given reaction rate, δ depends on the membrane permeability P, the membrane thickness l, and the tube reactor diameter d (inversely proportional to its surface-to-volume ratio). The membrane permeability is controlled by the nature of the membrane material. For proton-conducting membranes based on $SrCeO_3$ or $SrZrO_3$ perovskites, which are well suited for methane pyrolysis applications (Schober, Friedrich, & Condon, 1995; Hamakawa et al., 1993; Hamakawa et al., 1994; Borry et al., 1998), H_2 permeabilities are 10^{-13}–10^{-12} mol m^{-1} s^{-1} Pa^{-1} at 1000 K. The rate constant for CH_4 conversion on Mo/H-ZSM5 is k_1 which is 4×10^{-2} s^{-1} at 950 K. Thus, for a reactor diameter of 1 cm, the thickness of the membrane walls must be 10–100 μm in order to achieve δ values of 1–10. Recently, we have achieved the synthesis of such membrane films supported on porous substrates for $SrZr_{0.95}Y_{0.05}O_{3-\alpha}$ (Lu, 1999) and $SrCe_{0.95}Yb_{0.05}O_{3-\alpha}$ (Hamakawa, Li, Li, & Iglesia, 2002).

4. Conclusions

The nature of rate-determining steps in methane homogeneous pyrolysis sequences was explored in order to identify specific catalytic steps required to overcome the significant kinetic barriers inherent in purely homogeneous pyrolysis pathways. Catalytic sites that increase ethene to benzene conversion lead to higher methane conversion rates by removing the thermodynamic and kinetic inhibition effects caused by the increasing concentration of the H_2 formed in CH_4 reactions. Such sites, however, do not influence reaction rates in the chain transfer regime, within which homogeneous methane conversion pathways to form ethene limit overall reaction rates. Therefore, a catalyst that activates C–H bonds in CH_4 (and in any larger alkanes or alkenes), recombines CH_x groups to form C_2 hydrocarbons, and oligomerizes and cyclize alkenes into aromatics is required. Mo/H-ZSM5 catalysts appear to satisfy all of these requirements, but CH_4 conversion and hydrocarbon yields are limited by unfavorable reaction thermodynamics. A simplified consecutive reaction scheme using rate equations measured on Mo/H-ZSM5 were used in order to simulate the effects of H_2 removal on methane conversion rates and product selectivities. Simulation results suggest that bifunctional catalysts, such as Mo/H-ZSM5, with continuous H_2 removal can lead to almost complete CH_4 conversion at practical residence time (~ 100 s) and intermediate values of dimensionless transport rates ($\delta = 1$–10). For currently available membrane materials however, such δ values require 10–100 μm dense ceramic membrane films; the successful synthesis of such films has recently been reported.

Notation

C_i	Concentration of component i, mol m^{-3}
Da	Damkohler number
d	inner diameter of reactor, m
F_{j0}	mole feed flow rate of component j, mol m^{-2} s^{-1}

f_i	dimensionless rate expression for reaction i
J_{H_2}	hydrogen flux across the membrane, mol m^{-2} s^{-1}
K_j	equilibrium constant for reaction j
k_i	rate constant of reaction i
k_{h1}	CH_4 homogeneous activation rate constant, s^{-1}
k_{s1}	CH_4 catalytic activation rate constant, s^{-1}
L	reactor length, m
l	membrane thickness, m
P_j	permeability of component j through membrane, mol m^{-1} Pa^{-1} s^{-1}
P_f	permeability of fast component, mol m^{-1} Pa^{-1} s^{-1}
P_T	total pressure, Pa
p_{pm}	partial pressure of component j, Pa
q_j	dimensionless flow rate of component j in permeate side, mole flow rate/mole feed flow rate
R_j	formation rate of component j, mol m^{-3} s^{-1}
T	temperature, K
y_{jt}	mole fraction of component j on tube side
y_{js}	mole fraction of component j on shell side

Greek letters

α	permeability ratio, defined by Eq. (7)
β	reaction rate constant ratio, defined by Eq. (8)
γ	rate constant ratio
δ	ratio of permeation rate to reaction rate, defined by Eq. (6)
η_i	approach to equilibrium parameter, defined by Eqs. (12), (13) and (22)
λ_{ij}	stoichiometric coefficient for species j in reaction i
ξ	dimensionless axial distance
ρ	rate constant ratio between catalytic and homogeneous activation of CH_4
ϕ_j	dimensionless flow rate of component j in reaction side, molar rate/mole feed rate

Acknowledgements

This work was supported by the Division of Fossil Energy of the United States Department of Energy (Contract DE-AC03-76SF00098) under the technical supervision of Dr. Daniel Driscoll. The authors gratefully acknowledge Drs. Anthony M. Dean and Sebastian C. Reyes of ExxonMobil Research and Engineering and Professor Michael Frenklach of the University of California at Berkeley for their help with the homogeneous kinetic model and the thermodynamic data used in these simulations.

References

Andersen, A., Dahl, I. M., Jens, K.-J., Rytter, E., & Slagtern, A. (1989). Hydrogen acceptor and membrane concepts for direct methane conversion. *Catalysis Today*, *4*, 389–397.

Borry, R. W. (1998). *Non-oxidative methane conversion of Mo/H-ZSM5 catalysts for use in a hydrogen-transport membrane reactor*. Ph.D. dissertation, University of California at Berkeley.

Borry, R. W., Kim, Y.-H., Huffsmith, A., Reimer, J. A., & Iglesia, E. (1999). Structure and optimal density of Mo and acid sites in bifunctional Mo/H-ZSM5 methane aromatization catalysts. *Journal of Physical Chemistry B*, *103*, 5787.

Borry, R. W., Lu, E. C., Kim, Y. H., & Iglesia, E. (1998). Non-oxidative catalytic conversion of methane with continuous hydrogen removal. In A. Parmaliana, et al. (Eds.), *Studies in Surface Science and Catalysis*, Vol. 119 (pp. 403–410). Amsterdam: Elsevier.

Chen, L. Y., Lin, S. T., Xu, Z., & Zhang, T. (1995). *Journal of Catalysis*, *157*, 190.

Dean, A. M. (1990). Detailed kinetic modeling of autocatalysis in methane pyrolysis. *Journal of Physical Chemistry*, *94*, 1432–1439.

Ding, W. P., Li, S. Z., Meitzner, G. D., & Iglesia, E. (2001). Methane conversion of aromatics on Mo/H-ZSM5 structure of molybdenum species in working catalyst. *Journal of Physical Chemistry B*, *105*, 506–513.

Hamakawa, S., Hibino, T., & Iwahara, H. (1993). Electrochemical methane coupling using protonic conductors. *Journal of the Electrochemical Society*, *140*(2), 459.

Hamakawa, S., Hibino, T., & Iwahara, H. (1994). Electrochemical hydrogen permeation in a proton-hole mixed conductor and its application to a membrane reactor. *Journal of the Electrochemical Society*, *141*(7), 1720–1725.

Hamakawa, S., Li, L., Li, A., & Iglesia, E. (2002). Synthesis and hydrogen permeation properties of membranes based on dense $SrCe_{0.95}Yb_{0.05}O_{3-x}$ thin films. *Solid State Ionics*, *48*, 71–81.

Ito, T., & Lunsford, J. H. (1985). Synthesis of ethene and ethane by partial oxidation of methane over lithium-doped magnesium oxide. *Nature*, *314*, 721–722.

Jiang, Y., Yentekakis, I. V., & Vayenas, C. G. (1994). Methane to ethene with 85% yield in a gas recycle electrocatalytic reactor-separator. *Science*, *264*, 1563–1566.

Kee, R. J., Rupley, F. M., & Miller, J. A. (1990). *CHEMKIN—II: A FORTRAN chemical kinetics package for the analysis of gas-phase chemical kinetics*. Sandia Report SAND89-8009, UC-401, Sandia, NM.

Keller, G. E., & Bhasin, M. M. (1982). Synthesis of ethene via oxidative coupling of methane. I. Determination of active catalysts. *Journal of Catalysis*, *73*, 9–19.

Kim, Y.-H., Borry, R. W., & Iglesia, E. (2000). The genesis and catalytic properties of Mo-exchanged H-ZSM5. *Microporous Materials*, *35/36*, 495.

Labinger, J. A. (1988). Oxidative coupling of methane: An inherent limit to selectivity. *Catalysis Letters*, *1*, 371–375.

Langguth, J., Dittmeyer, R., Hofmann, H., & Tomandl, G. (1997). Studies on oxidative coupling of methane using high-temperature proton-conducting membranes. *Applied Catalysis A: General*, *158*, 287–305.

Li, L., Borry, R. W., & Iglesia, E. (2001). Reaction-transport simulations of non-oxidative methane conversion with continuous hydrogen removal: Homogeneous–heterogeneous methane reactions. *Chemical Engineering Science*, *56*(5), 1869–1881.

Lu, E. C. (1999). *Non-porous hydrogen-selective inorganic membranes for methane conversion to higher hydrocarbons*. Master thesis, University of California at Berkeley.

Lunsford, J. H., Rosynek, M. P., & Wang, D. (1995). In *Proceedings of fourth international natural gas symposium*, Kruger National Park, South Africa.

Reyes, S. C., Iglesia, E., & Kelkar, C. P. (1993). Kinetic-transport models of bimodal reaction sequences—I. Homogeneous and heterogeneous pathways in oxidative coupling of methane. *Chemical Engineering Science*, *48*(14), 2643–2661.

Schober, T., Friedrich, J., & Condon, J. B. (1995). Effective hydrogen diffusivity in $SrCe_{0.95}Yb_{0.05}O_{3-\alpha}$ and $SrZr_{0.95}Y_{0.05}O_{3-\alpha}$. *Solid State Ionics*, *77*, 175–179.

Solymosi, F., Cserenyi, J., Szoke, A., Bansagi, T., & Oszko, A. (1997). Aromatization of methane over supported and unsupported Mo-based catalysts. *Journal of Catalysis*, *165*, 150–161.

Solymosi, F., Erdohelyi, A., & Szoke, A. (1995). Dehydrogenation of methane on supported molybdenum oxides. *Formation of benzene from methane*, *Catalysis Letters*, 32.

Tonkovich, A. L., Carr, R. W., & Aris, R. (1993). Enhanced C_2 yields from methane oxidative coupling by means of a separative chemical reactor. *Science*, *262*, 221–223.

Wang, D., Lunsford, J. H., & Rosynek, M. P. (1996). Catalytic conversion of methane to benzene over Mo/ZSM5. *Topics in Catalysis*, *3*, 289–297.

Wang, L., Tao, L., Xie, M., & Xu, G. (1993). Dehydrogenation and aromatization of methane under non-oxidizing conditions. *Catalysis Letters*, *21*, 35–41.

Woldman, L. S., & Sokolovskii, V. D. (1991). Electrocatalytic methane coupling in the absence of oxygen on a high-temperature proton-conducting electrolyte. *Catalysis Letters*, *8*, 61–66.